

Signal Processing Based Deep Learning for Blind Symbol Decoding and Modulation Classification

Samer Hanna, *Student Member, IEEE*, Chris Dick, *Senior Member, IEEE*, and Danijela Cabric, *Fellow, IEEE*

Abstract—Blindly decoding a signal requires estimating its unknown transmit parameters, compensating for the wireless channel impairments, and identifying the modulation type. While deep learning can solve complex problems, digital signal processing (DSP) is interpretable and can be more computationally efficient. To combine both, we propose the dual path network (DPN). It consists of a signal path of DSP operations that recover the signal, and a feature path of neural networks that estimate the unknown transmit parameters. By interconnecting the paths over several recovery stages, later stages benefit from the recovered signals and reuse all the previously extracted features. The proposed design is demonstrated to provide 5% improvement in modulation classification compared to alternative designs lacking either feature sharing or access to recovered signals. The estimation results of DPN along with its blind decoding performance are shown to outperform a blind signal processing algorithm for BPSK and QPSK on a simulated dataset. An over-the-air software-defined-radio capture was used to verify DPN results at high SNRs. DPN design can process variable length inputs and is shown to outperform relying on fixed length inputs with prediction averaging on longer signals by up to 15% in modulation classification.

Index Terms—blind symbol decoding, deep learning, automatic modulation classification

I. INTRODUCTION

In a typical wireless communication system, the transmitter and receiver exchange waveforms following an agreed upon protocol. However, a prior agreement on waveforms is not always possible and heterogeneous radios might need to communicate without a protocol predefining waveforms. Without a known protocol, a blind receiver has to reconstruct and decode an unknown waveform in many applications. Civilian applications include decoding unknown signals to enable exchanging messages between heterogeneous radios using dynamic spectrum access. Military applications of blind decoding include intercepting hostile communications.

Decoding a blindly received signal is a challenging problem. In addition to all the channel impairments facing protocol based communications, a blind receiver lacks any knowledge about the transmitted signal. Without an agreed upon preamble for synchronization and channel estimation and without knowing the type of modulation, a blind receiver has only access to a sequence of IQ samples representing unknown symbols. From

this sequence, the receiver needs to figure out the symbol rate, the modulation type, the channel impulse response for equalization, and compensate for carrier and timing synchronization errors to recover the transmitted symbols. Additionally, the length of a blindly received signal is not determined a priori.

While it is easy to generate signals of different parameters and channel distortions, developing signal processing algorithms that jointly estimate all these parameters for blind decoding is more challenging. Many existing works have leveraged blind signal processing to address blind decoding and modulation classification [1]–[3]. However, these works address the estimation problems separately, thus, not benefiting from joint estimation, and many of them make assumptions impractical for a blind receiver like assuming synchronization.

Driven by the availability of training data, some of the estimation problems in blind decoding were separately addressed using deep learning; Center frequency and timing offset estimation neural networks were proposed in a non-blind context for QPSK signals [4]. For modulation classification, deep neural networks were shown to outperform manually designed features in [5]. However, posing blind decoding as a set of independent deep learning estimations has its drawbacks. It does not allow the networks to share common features and thus prevents them from performing joint estimation by learning the dependencies between the parameters present in the signal. It also denies each network benefiting from the other networks' outputs, which can partially recover the signal and reduce distortions. To avoid these limitations, another option is an end-to-end deep learning solution taking the signal as input and outputting the symbols.

Using a black box end-to-end neural network for blind decoding also has its drawbacks. Unlike modulation classification or estimation, blind decoding needs to be applied to the entire length of the signal and thus needs to be efficiently scalable. Deep learning can have a high computational complexity compared to digital signal processing (DSP) and lacks interpretation [6]. For efficient scaling, estimating the unknown parameters and relying on DSP for compensation can be more computationally efficient than relying on an end-to-end black box neural network. Additionally, interpretable outputs can easily be integrated with existing DSP techniques. The drawbacks of separate estimations and end-to-end solutions motivate for a model-based deep learning solution [7], integrating both signal processing and deep learning in a design combining the benefits of both.

Another common limitation of neural networks used in many existing works addressing similar problems is the fixed input size. For instance, in [5], it was shown that neural

Samer Hanna and Danijela Cabric are with the Electrical and Computer Engineering Department, University of California, Los Angeles, CA 90095, USA. Chris Dick is with Nvidia Inc. and was at Xilinx Inc. San Jose, California, USA when this work started e-mails: samerhanna@ucla.edu, cdick@nvidia.com, danijela@ee.ucla.edu

This work was supported in part by the CONIX Research Center, one of six centers in JUMP, a Semiconductor Research Corporation (SRC) program sponsored by DARPA.

networks using longer signals can lead to improved modulation classification accuracy. However, the proposed networks can only process fixed length signals and network redesign and re-training is required to change the input length. Blind receivers do not have control over the received signal length and it is not practical to train a separate network for each possible signal length. To use fixed length networks on variable size inputs, one approach is to train them on short signals and divide longer signals into chunks and use averaging as proposed in [8]. Another approach, which provides more flexibility, is to design the neural networks that handle variable length signals as proposed in [9], [10]. However, it is not clear which approach yields a better performance.

In this paper, we propose the Dual Path Network (DPN) for blind decoding and modulation classification. To overcome the limitations of separate estimations and end-to-end networks, the dual path network is designed as two paths; a signal path and a feature path. The signal path consists of linear signal processing operations where frequency offset, noise, and fading are compensated for sequentially. The feature path consists of neural networks that process the features extracted from the input and the compensated signals. These features are used to predict interpretable signal processing estimates and filter taps. Using this architecture, DPN benefits from recovered signals and can combine features from all stages. Once the estimates have been obtained, due to their signal processing interpretation, they can be integrated with existing signal processing techniques. By leveraging average pooling and recurrent networks to obtain the predictions, DPN can process variable length inputs. Our contributions can be summarized as follows

- We propose the Dual Path Network (DPN) architecture for blind signal decoding, which can process inputs of variable lengths. DPN design integrates signal processing with neural networks yielding interpretable outputs. The proposed architecture enables learning from recovered signals and allows features combining.
- We verify the benefit of learning from recovered signals and combining features along the signal path. To do that, we compare DPN to alternative architectures that lack access to either recovered signals or feature combining and show that DPN outperforms either architecture by up to 5% in modulation classification.
- For inference on variable length, we show that using DPN trained and tested with variable lengths provides lower estimation errors and up to 15% improvement in modulation classification compared to averaging the predictions calculated using the same network trained and tested only using a short fixed input size.
- We show that DPN provides lower estimation errors and a higher percentage of correctly decoded signals for BPSK and QPSK on the test dataset compared to an implemented blind signal processing algorithm.

II. RELATED WORK

In section, we start by discussing existing signal processing approaches for blind decoding, then we survey the deep

learning approaches used for problems that are part of blind decoding. Works that have considered deep learning demodulators are discussed last.

a) DSP approaches for Blind Decoding: Blind decoding DSP approaches rely on recovering the symbols then analyzing them to identify the modulation types. In [1], cyclostationary features were used for carrier frequency offset and symbol rate estimation to recover the symbols. Using the recovered symbols, a decision tree algorithm based on statistical tests for blind modulation classification was proposed. Assuming synchronization in an AWGN channel, joint modulation classification and symbol decoding were performed using two approaches based on a Bayesian framework and a minimax framework in [2]. Under the assumption of perfect synchronization, in [3], an iterative approach was proposed for joint blind channel estimation, modulation classification, channel coding recognition, and data detection using a different approach for each task.

b) Deep Learning Approaches for Estimation and Modulation Classification: Many deep learning approaches were proposed for problems relevant to blind decoding. Deep learning was proposed for carrier frequency offset and timing offset estimation and was compared to traditional estimators in [4]. In [11], deep learning from raw IQ samples was shown to outperform manually designed features in the problem of modulation classification. This result sparked a wide interest in developing novel modulation classification neural network architectures. In [5], a residual neural network was proposed and the effects of fading and frequency offsets were studied. Recurrent neural networks were proposed for modulation classification in [12] and were shown to outperform convolutional networks. A network combining both CNN and LSTM networks was proposed in [13]. In [14], branch convolutional neural networks, consisting of a hierarchy of neural networks were used to classify 29 modulation types. A network design that combines shallow and high level features of the input signals was proposed in [15]. In [16], a cyclic connected CNN along with a bidirectional RNN were proposed. Instead of using IQ samples, the signals to be classified were represented as constellation images in [17]–[20]. Other works have focused on designing lightweight networks that reduce the number of parameters or the inference time [10], [21]–[26]. Modulation classification was also considered for multi-carrier signals in [27] and for MIMO systems in [28], [29]. In [9], [30], distributed modulation classification using multiple receivers to capture the same signal was proposed.

Deep learning was shown to be affected by synchronization errors, which motivated the development of custom signal processing layers. The effects of carrier frequency offsets and sampling offsets on modulation classification were studied in [31]. It was shown that frequency offsets and sampling rate offsets degrade the classification accuracy with the former having a more pronounced effect. Driven by this observation, custom neural network layers that attempt to recover the signal before classification were proposed. A spatial transformer network was proposed in [32] for timing recovery and was shown to improve accuracy at low oversampling. In [33], a radio transformer network that can correct frequency offset and

adjust the sampling rate of the signal was proposed. Similarly, a learnable distortion correction module for frequency and phase offset was proposed in [34]. In [35], a U-net network was proposed to reconstruct low SNR signals. In these works, the custom reconstruction layers were trained to improve the modulation classification results without the reconstruction ground truth, and hence are not guaranteed to recover the transmitted signals. Thus, the output of such networks can not be used for blind decoding.

Most of the neural network architectures in the literature were designed only to process signals with a fixed length input. To use a fixed length network on a signal with a different length, the network has to be redesigned and retrained. To extend a network to longer signals without retraining, in [8], the authors have proposed methods to combine the predictions applied on small chunks of a signal. These methods consist of averaging the predictions. Neural networks that can process variable input size signals were proposed by using LSTM in [9] and by combining convolutional layers and average pooling in [10]. However, it is still not clear which network design yields a higher accuracy on signals of length unseen in training; a fixed length network with combined predictions or a variable length network.

c) Deep Learning Approaches for non blind Demodulation: Several works have proposed using deep learning for demodulation when the transmitter signal parameters are known a priori. In [36], an end-to-end neural network demodulator was developed under the assumption of time synchronization between the transmitter and receiver. Several modulation types were supported and a network was trained for each type. For WiFi, neural networks were proposed to replace several signal processing blocks of a WiFi receiver in [37]. These blocks include channel estimation, phase error correction, sampling rate correction, and equalization and rely on the WiFi preambles to perform their tasks. A similar approach was proposed for 5G compliant waveforms in [38]. Deep learning end-to-end communications systems, where both the transmitter and receivers are neural networks, were also proposed. In [39] and [40] autoencoders were proposed for SISO communications and in [41] for MIMO. These approaches, however, rely on knowing or designing the transmitted signal and do not directly apply to blind decoding.

The dual path network was first introduced in our prior work [42], which we extend in this work. In this work, DPN design and training process was improved as discussed later. A more thorough evaluation was performed to evaluate the effect of signal reconstruction and feature sharing among different stages. The blind decoding performance was compared with both blind and Genie signal processing approaches. An over-the-air capture was used to validate our results. DPN was evaluated on variable input lengths and different approaches for variable length training and inference were considered.

III. SYSTEM MODEL AND PROBLEM FORMULATION

We start by describing the system model and the underlying assumptions of our work. A transmitter sends a vector of complex symbols $\mathbf{s} \in \mathbb{C}^{N_s}$ using modulation type M from a set

of modulations \mathcal{M} . In the most general case, the transmitted signal $x(t)$ is determined by symbols \mathbf{s} and symbol duration τ through a modulation specific mapping function \mathcal{G} such that $x(t) = \mathcal{G}(\mathbf{s}, \tau)$. For a linear modulation type, each symbol s_i represents a mapping from bits to a constellation point, and the transmitted signal $x(t)$ is given by $x(t) = \sum_{i=1}^{N_s} s_i p(t - i\tau)$ where $p(t)$ is the pulse shaping filter. The signal is upconverted and transmitted over a multipath fading channel modeled with an impulse response $h(t)$ having a delay spread σ . At the receiver, the downconverted and sampled signal is modeled using the vector $\mathbf{y} \in \mathbb{C}^{N_r}$ with the k -th element given by

$$y[k] = e^{j2\pi(f_0 t_k + \phi_0)} \int_{-\infty}^{\infty} x(\gamma) h(t_k - \gamma) d\gamma + n(t_k) \quad (1)$$

where f_0 is the carrier frequency offset, ϕ_0 the phase offset, and $n(t)$ is the additive white Gaussian noise process with zero mean and power spectral density $N_0/2$. We assume that the receiver sampling rate is given by $\frac{1}{\tau_0}$. The sampling instance of the k th sample is given by $t_k = t_0 + k\tau_0$, where $\tau_0 \leq \tau$ and t_0 is the symbol timing offset. The length of the transmitted symbols N_s and the received IQ samples N_r are related using $N_r = N_s \left\lceil \frac{\tau}{\tau_0} \right\rceil$. Such signals can be captured using a narrowband receiver coarsely tuned to the center of a spectrum occupancy or using a wideband receiver followed by coarse band segmentation. Either way, we assume that the vector \mathbf{y} contains only one signal and that the sampling satisfies the Nyquist criterion. The parameters f_0, ϕ_0, h are assumed to be constant along the duration of each signal.

To avoid dependence on hardware specifications that vary from one radio to the other, we normalize the previous parameters with respect to the sampling rate. This is done by using the frequency normalized to the sampling rate $\frac{f_0}{1/\tau_0}$, the number of samples per symbol $\frac{\tau}{\tau_0}$, and the normalized timing offset $\frac{t_0}{\tau_0}$. Without loss of generality, to simplify the notation, we consider $\tau_0 = 1$, which is equivalent to assuming a 1Hz sampling rate. Under this assumption, the number of samples per symbol τ becomes equal to the symbol duration.

The problem considered is described as follows: Given the vector \mathbf{y} , the receiver's objective is to identify the modulation type M among the set of modulations \mathcal{M} and recover the transmitted symbols \mathbf{s} .

IV. DUAL PATH NETWORK (DPN)

The main ideas behind the dual path network design are: (1) the less the distortions, the better the predictions, (2) Estimating jointly is better than separately. If the receiver had access to the transmitted signal, $x(t)$, the considered problem would have been easier. Using this idea, to improve its predictions, DPN attempts to recover the signal $x(t)$. The signal recovery is inspired by existing DSP techniques, which rely on knowing the signal parameters (symbol rate, modulation type, etc.) [43], [44]. To overcome the ignorance of these parameters, the dual path network uses neural networks to predict the values for the compensation. These networks are designed to enable joint estimation by maximizing the feature sharing among them.

Feature Path

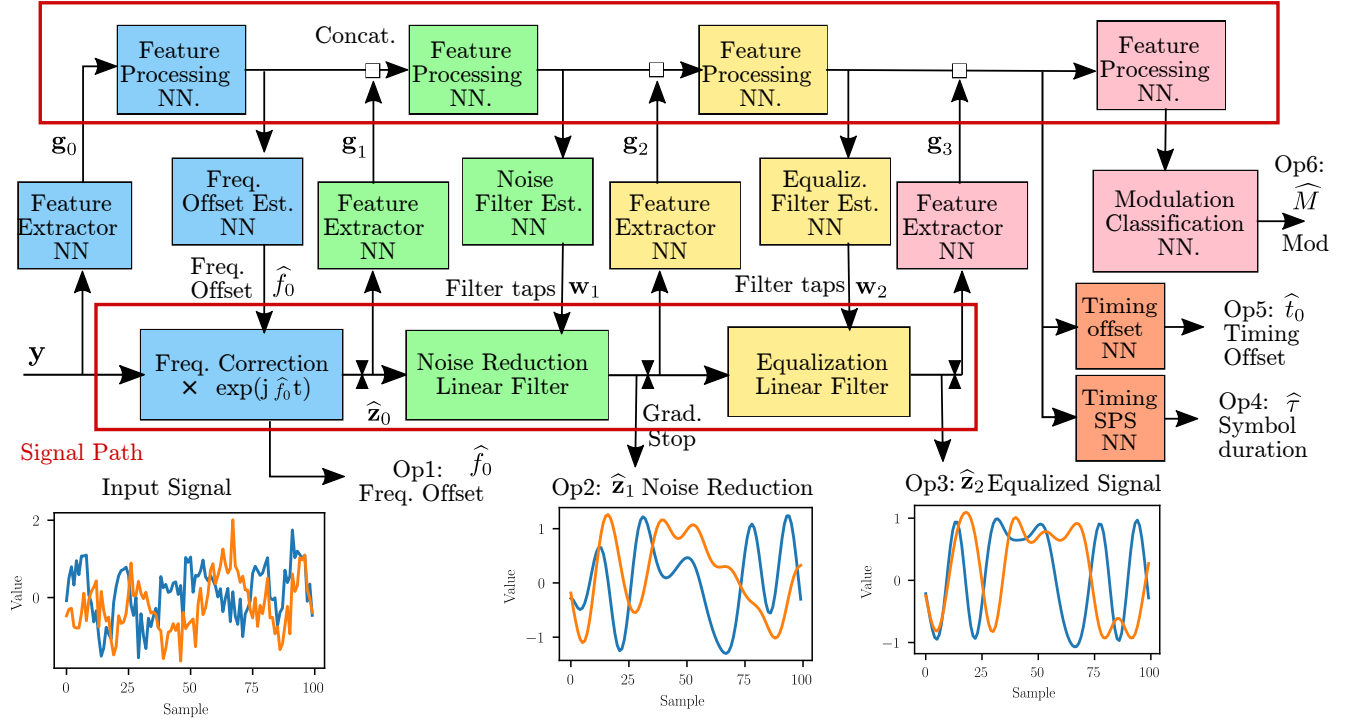


Fig. 1: The Dual Path network consists of feature path and a signal path connected using neural networks (NN) for parameter estimation and feature extraction. A slice of an example input signal and expected outputs of the network are plotted.

A. Dual Path Design

The proposed network consists of two paths: a signal path consisting of linear operations that gradually restore the input signal, and a feature path made of neural networks (NN) used to predict the parameters needed to recover the transmitted signal. The network is shown in Fig. 1. The signal path is described as follows: It starts by compensating for the frequency offset using the network's prediction \hat{f}_0 , to obtain the vector \hat{z}_0 defined as

$$\hat{z}_0[k] = y[k]e^{-j2\pi\hat{f}_0k} \quad (2)$$

The noise of the signal is then attenuated using the predicted real filter taps \mathbf{w}_1 and generates the vector \hat{z}_1 defined as

$$\hat{z}_1[k] = \hat{z}_0[k] * w_1[k] \quad (3)$$

where $*$ denotes the linear convolution operator. At the end of the signal recovery, equalization is performed using the predicted complex filter taps \mathbf{w}_2 , to generate the vector \hat{z}_2 defined as

$$\hat{z}_2[k] = \hat{z}_1[k] * w_2[k] \quad (4)$$

Note that due to linearity, both filtering stages can be combined, and a single set of predicted filters can perform both operations. However, we decided to keep the two filters separate similar to our prior work [42] to make training easier and for the network to extract features from two recovered signals instead of one.

Feature Extractor NNs extract the features vectors \mathbf{g}_0 , \mathbf{g}_1 , \mathbf{g}_2 , and \mathbf{g}_3 from the signals y , \hat{z}_0 , \hat{z}_1 , and \hat{z}_2 respectively. Each of these feature vectors is concatenated with the processed

previous features along the feature path, which consists of 4 cascaded Feature Processing neural networks (NNs) as shown in Fig. 1. The predicted parameters used by the signal path \hat{f}_0 , \mathbf{w}_1 , and \mathbf{w}_2 along with predictions of the timing offset \hat{t}_0 , symbol duration $\hat{\tau}$, and the modulation type \hat{M} are obtained by their own dedicated estimation neural networks. The layer by layer description of the networks is discussed later in Section IV-E. The recovery of the symbols \mathbf{s} is performed using these parameters in post processing as described later in Section V-B.

B. Design Motivation and Considerations

In this section, we explain the motivation behind DPN design. The sequential stage by stage design enables later stages to benefit from the output of earlier stages. The stage order is chosen based on the effect of the distortion on the signal time domain representation. A small frequency offset can significantly alter the signal in time domain even at a high SNR, so it was considered first. Frequency recovery is also typically the first stage in classical demodulators [43]. For limited fading spread, the noise has a more pronounced effect on the signal, and it was considered as the second stage. However, other stage orders are possible; for instance, in our prior work [42], the noise reduction stage was first due to a different choice of training data. The training data used in DPN is discussed later in Section IV-D.

Besides the 3 recovery stages, other DSP operations need to be performed to recover the symbols, however, there are design considerations that prevent integrating them into DPN. The first consideration is that all operations in DPN have to

be differentiable to train it using gradient descent. The second consideration is that the output size needs to be determined only by the input size and should not depend on the network predictions. Although there are known techniques to train NN that violate this consideration (commonly used in natural language processing), this consideration makes training easier. The third consideration is that the network should not be penalized for phase ambiguity. For example, if a signal $x(t)$ is a valid BPSK signal, $-x(t)$ is also a valid BPSK signal. Since the network does not have sufficient information to determine the correct one, it should not be penalized.

These considerations make it hard to design a network that uses DSP modules to output the N_s symbols \mathbf{s} for several reasons; (1) the relation between the signal length N_r and N_s depends on the number of samples per symbol τ , which is unknown and varies from one training sample to the other, (2) the number of possible values of each output symbol is also a variable that depends on the modulation order, (3) considering phase ambiguity, there are several possible valid values of the sequence symbols. So instead of designing a network that outputs \mathbf{s} directly, we design a network that recovers the transmitted signal and estimates the parameters needed to decode \mathbf{s} , which is done in post-processing.

C. Design Merits and Drawbacks

The proposed DPN design combining neural networks and signal processing has several merits:

- 1) *Predicting using restored signals*: The less the distortions in the signal (higher SNR, smaller frequency offsets, etc.), the better the predictions that neural networks obtain [31]. DPN design gradually restores the transmitted signal and uses the restored signal in the later predictions. This should lead to improved predictions.
- 2) *Incremental Feature Combining*: Each prediction made by the network has access to all features from the previous stages. For instance, the modulation classification NN, through the feature path can leverage all the previous features \mathbf{g}_1 , \mathbf{g}_2 , \mathbf{g}_3 , and \mathbf{g}_4 not just \mathbf{g}_4 . The combining enables any prediction NN block to reuse relevant features from the previous stages. It also works as a backup in case a signal reconstruction stage leads to degradation in the signal due to misprediction, which might occur at low SNR.
- 3) *Compatibility with Existing DSP Methods*: The DPN outputs are frequency estimates, filter taps, and timing estimates. All these parameters have a clear interpretation and can be reused using existing signal processing techniques. For instance, if the received signal is too long, DPN can be applied to obtain estimates on a short portion of the signal. The estimates like frequency offset can be directly applied to the remaining signal. In case there exists a time varying frequency drift, a frequency offset tracking algorithm can be applied to DPN's estimate.

All three claimed merits are verified in the results section. To verify the first two merits, we consider two alternative designs of DPN, which are described later in Section IV-G.

TABLE I: Loss Functions

Equation
$L_1 = \hat{f}_0 - \tilde{f}_0 $
$L_2 = \frac{1}{N_r} (\hat{\mathbf{z}}_1^H \tilde{\mathbf{z}}_1 + \mathbf{z}_1^H \mathbf{z}_1 - 2 \hat{\mathbf{z}}_1^H \mathbf{z}_1)$
$L_3 = \frac{1}{N_r} (\hat{\mathbf{z}}_2^H \tilde{\mathbf{z}}_2 + \mathbf{z}_2^H \mathbf{z}_2 - 2 \hat{\mathbf{z}}_2^H \mathbf{z}_2)$
$L_4 = (\hat{t}_0 - t_0)^2$
$L_5 = (\hat{\tau} - \tau)^2$
$L_6 = \text{crossentropy}(M, \hat{M})$

The design of DPN also has several drawbacks. Since the signal path consists only of linear operations, DPN can only perform linear reconstruction of the signal, that is the reconstructed output $\hat{\mathbf{z}}_2$ is obtained using linear operations on the input \mathbf{y} . This is in contrast with using a fully neural network design which can approximate non linear relations between its input and output. However, non linear distortions are typically mitigated in the radio hardware design, and communication systems are typically modeled using linear operations. The second drawback is that training DPN requires different types of data for training. DPN requires the true value of many signal parameters like frequency and timing offsets in addition to \mathbf{y} . However, these parameters are easy to obtain in a simulator. To train DPN with an over the air capture, a long preamble can be used to precede known transmitted signals. Using existing signal processing techniques, the channel, the frequency, and timing offsets can be estimated to obtain the required training data.

These previous merits and drawbacks are specific to the proposed design. DPN also inherits some of the merits and drawbacks of deep learning. DPN predicts using the weights calculated in training instead on relying on manually designed features. This data driven approach makes it relatively easy to support another modulation type for instance at the cost of lacking an interpretation of what is being learned.

D. Training Data and Method

DPN is trained using stochastic gradient descent. The labeled data used in training consists of received signals \mathbf{y} along with their corresponding values f_0 , \mathbf{z}_1 , \mathbf{z}_2 , t_0 , τ , and M , where \mathbf{z}_1 is the noise free received signal

$$z_1[k] = \int_{-\infty}^{\infty} x(\gamma)h(t_k - \sigma)d\gamma \quad (5)$$

and \mathbf{z}_2 is the noise free and equalized signal

$$z_2[k] = x(t_k) \quad (6)$$

Since, we are including the values of f_0 , \mathbf{z}_1 , \mathbf{z}_2 , the reconstruction stages are trained in a supervised manner. To evaluate the feasibility omitting the signal ground truth in blind decoding similar to [32]–[35], we consider an unsupervised-reconstruction alternative architecture as discussed later in Section IV-G. Other choices of the training data are possible. For instance, instead of using \mathbf{z}_1 and \mathbf{z}_2 , we could have designed a low pass filter \mathbf{w}_1 and an equalization filter \mathbf{w}_2 and used them for training. Since there are many possible

ways to design these filters, instead of forcing the network to a specific design, we opted for only including the desired outputs \mathbf{z}_1 and \mathbf{z}_2 in the training. Also instead of using f_0 for training, we could have used a reference signal with no offset similar to what we did in our prior work [42], but explicitly using f_0 was found to provide a better reconstruction. Since we are providing the ground truth along the signal path, and to avoid confusing the estimation networks, gradients were prevented from propagating along the signal path according to the gradient stops shown in Fig. 1.

Since the outputs are heterogeneous, each output has its own loss function as defined in Table I. For the modulation type, the classifier was trained using the categorical crossentropy loss. For the frequency and timing predictions, we used the mean absolute error and the mean square error respectively. A natural choice for \mathbf{z}_1 is the mean squared error (MSE) loss defined as $\frac{1}{N_r} \|\mathbf{z}_1 - \widehat{\mathbf{z}}_1\|^2 = \frac{1}{N_r} (\widehat{\mathbf{z}}_1^H \widehat{\mathbf{z}}_1 + \mathbf{z}_1^H \mathbf{z}_1 - 2\widehat{\mathbf{z}}_1^H \mathbf{z}_1)$, where $(\cdot)^H$ denotes the hermitian operator. However, this choice penalizes constant phase offsets, and thus violates our design consideration for phase ambiguity. To avoid penalizing constant phase offsets, we used the modified loss shown in Table I for L_2 and L_3 . It is easy to verify that $\widehat{\mathbf{z}}_1$ and $\widehat{\mathbf{z}}_1 e^{j\phi}$ for any phase ϕ would yield the same loss. Note that the modified loss used in L_2 and L_3 is still sensitive to residual frequency offsets $(\widehat{f}_0 - f_0)$, which are time varying phase offsets.

To support the feature combining along the feature path, DPN is trained simultaneously as a single network with a loss $L = \sum_{k=1}^6 c_k L_k$, for some weights c_k . This implies that the gradients for a given NN backpropagate from all the subsequent outputs. For instance, the weights of the first feature extractor (generating \mathbf{g}_0) are trained using gradients from all the outputs not just \widehat{f}_0 . This makes the weights of each NN along the feature path optimized to minimize the total loss and not the loss of a specific output.

E. Scalable Neural Network Architecture

We start by describing the building blocks of the network. The entire network consists of a combination of convolutional networks and recurrent neural networks. This choice was not only based on their outstanding results in modulation classification [5], [12], but also because their number of trainable parameters is independent from the input length [45, Ch.10]. A convolutional layer is based on the convolution operation, in which the number of trainable filter weights is independent of the input size. Similarly, a recurrent neural network uses the same weights for any number of time steps [45, Ch.10].

Then, we describe each network in details. The convolutional layers used in this work were arranged as residual blocks. Residual blocks improve the gradient flow during the training of deep networks [46] and were proposed for modulation classification [5]. The neural network blocks layer by layer descriptions are shown in Fig. 2. Both timing offset and symbol duration prediction used the same architecture referred to as Timing Est. The noise reduction filter used the Filter Est shown in the same figure. The fading filter used has complex taps, hence needs twice the number of real outputs. It was obtained by modifying the Filter Est block to have two

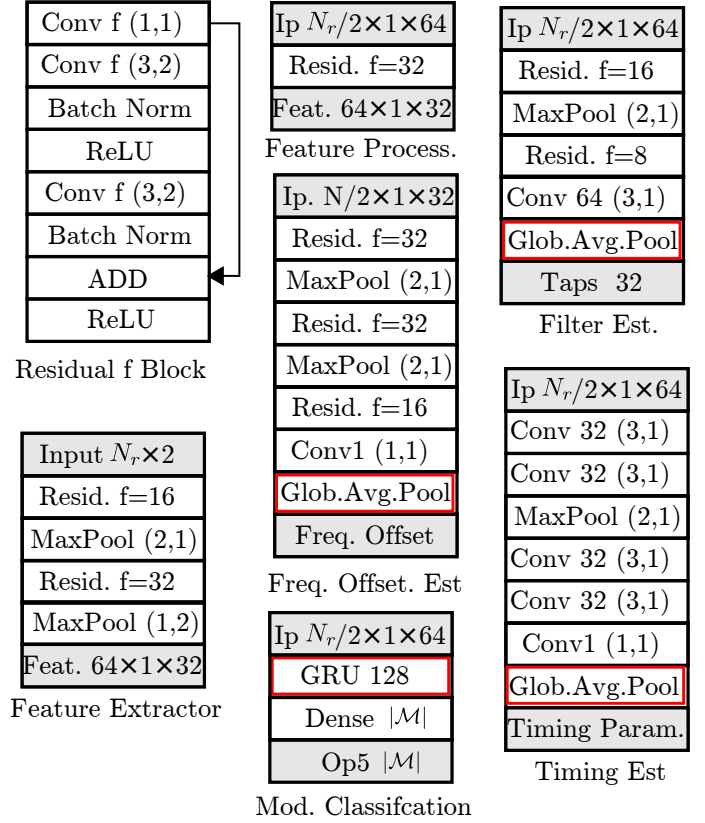


Fig. 2: The layer by layer description of the NNs in DPN.

32 sample outputs by duplicating the layers following the last residual block. The modulation classification block consists of a gated recurrent unit (GRU) network, which is a type of recurrent network followed by a dense layer.

To support variable length signals, all layers generating the network outputs either use global average pooling or recurrent neural networks. Global average pooling calculates the average along the time dimension. Hence, it does not have any trainable weights and is independent of its input time dimension. This is in contrast with most existing works, which rely on a dense network after the convolutions with the number of trainable weights dependent on the time dimension. The output of the recurrent network is obtained from the last time step and hence its output dimension is independent from the time dimension. The layers generating outputs independent of the time dimension are highlighted in red in Fig. 2.

DPN has a total of 233,419 trainable parameters. This number of parameters is independent of the input length N_r . No matter how long the input is, the number of weights is constant. However, the fact that the same weights can be reused for the different lengths does not imply that the performance will generalize across different lengths. We will explore the effect of changing the signal input length on the performance in our evaluation.

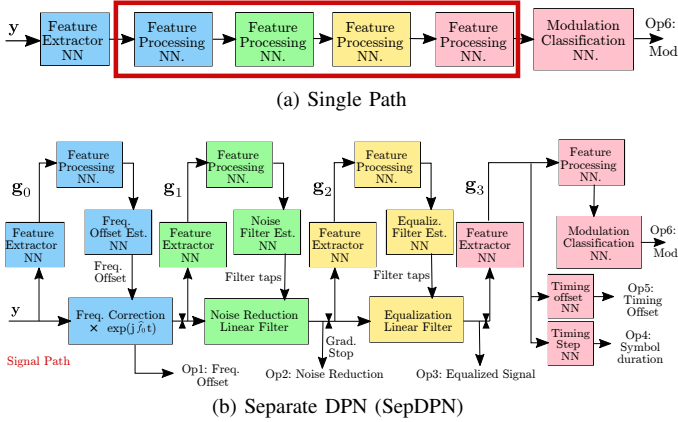


Fig. 3: Alternative DPN designs.

F. DPN Implementation and Training Parameters

The code for DPN is publicly available¹. DPN was implemented using the KERAS API for TensorFlow. It was trained for 100 epochs, with early stopping occurring if the validation loss did not improve for 10 consecutive epochs. The best weights according to the validation loss are retained. Note that early stopping is used to determine when the network weights have converged and not to avoid overfitting. Overfitting is avoided by using realtime signal generation as discussed later in Section VI.

The weights for the losses c_1 to c_6 were set to 500, 1, 5, $2.4e-4$, $4.8e-4$, 1.0 respectively. These values were chosen to account for the relative importance of the parameters and the different magnitudes of the losses which depend on the training labels values that are described later. For instance frequency offset loss (L_1) takes values in the range of $1e-2$, and has a large impact on blind decoding and modulation classification and hence was assigned a large weight $c_1 = 500$. In contrast, the timing offset loss (L_4) takes values in the range of 1K (when using integer sample offsets) and hence was assigned a small weight $c_4 = 2.4e-4$. The optimizer used for training is the ADAM optimizer with a learning rate of 0.001 and the gradients were clipped at a norm of 1.0 to avoid exploding gradients [47].

G. Alternative Architectures

We consider two alternative designs for DPN to verify some of the claimed merits and a third one to evaluate the benefit of supervised reconstruction. The first design aims to quantify the impact of restoring the signal on modulation classification. This design omits the signal path entirely from DPN as shown in Fig. 3a and is referred to as Single Path. If restoring the signal improves predictions as claimed, DPN should outperform Single Path in modulation classification.

The second alternative design aims to verify the benefits of feature combining. To prevent feature combining, the feature path is disconnected as shown in Fig. 3b preventing feature combining. Since the signal path contains gradient stops,

the gradients of one stage do not propagate to the previous stage and the stages are separate. This network referred to as Separate DPN (SepDPN) and is equivalent to training one stage, calculating the predictions, and using them to train the following stage. Hence, in this design, the features \mathbf{g}_0 are used exclusively for the prediction of \hat{f}_0 , and similarly for the later stages. If feature combining leads to an improvement in prediction as claimed, DPN should outperform SepDPN.

The third alternative considers the effect of training of the signal reconstruction stages without the ground truth similar to what was proposed in [32]–[35] for modulation classification. The design is similar to DPN design shown in Fig. 1 after omitting the ground truth values of f_0 , \mathbf{z}_1 , \mathbf{z}_2 , t_0 , and τ , leaving only the modulation type M . To train the network, the gradient stops along the signal path were removed. The timing networks were also omitted because they cannot be trained without the ground truth. This alternative design, referred to as unsupervised DPN (unsupDPN), investigates whether unsupervised reconstruction is valid for blind decoding or not. It also investigates the impact of supervised reconstruction on modulation classification.

V. SIGNAL RECOVERY AND SYMBOL DECODING ALGORITHM

In this section, we discuss the benchmark algorithms for signal recovery used for comparison. We also discuss DPN postprocessing and symbol decoding.

A. Benchmark Signal Recovery Algorithms

To evaluate the performance of DPN in signal recovery, we contrast it with exiting DSP techniques. To that end, we consider two algorithms; the first one is a fully blind recovery algorithm based on signal processing, the second is a genie algorithm that assumes all the unknown signal parameters are provided by a genie. It is important to note that there exist many signal processing algorithms for recovery whether blind or genie. These algorithms have a tradeoff between complexity and performance. The chosen algorithms were selected to be non-iterative and to rely on well known DSP techniques.

1) *Blind DSP Reference Algorithm (DSP Ref)*: The reference blind algorithm used is based on the symbol recovery proposed in [1]. It starts with band segmentation stage aiming to obtain an initial estimate of the signal center frequency and bandwidth. It is performed using the Welch power spectral density as described in Appendix A. The initial estimates are refined by detecting the signal's cyclostationary features as proposed in [1, Sec. III-B]. The exact refinement procedures are described in Appendices B and C for center frequency and symbol rate respectively. After the estimation of τ and f_0 , the timing offset t_0 is estimated using the Gardner symbol timing recovery algorithm [48] as described in Appendix D. The constant modulus algorithm (CMA) is then applied for blind signal equalization [49] as described in Appendix E.

2) *Genie Algorithm*: The genie algorithm assumes all the parameters which were used to generate the signal are known. It starts by correcting the frequency offset, then applying a low pass filter over its bandwidth, which are both assumed to be

¹https://github.com/uclacores/dual_path_network

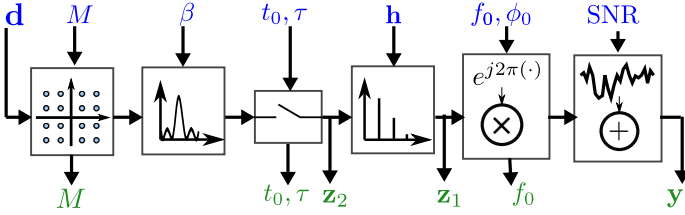


Fig. 4: Flow graph for generating samples showing on top the input parameters and the bottom the outputs used for training.

known. It uses the MMSE equalizer assuming that the channel is known as described in Appendix F. The symbol recovery is performed using the true τ and t_0 using the same procedures as DPN output, which are described in Section V-B.

B. DPN Post Processing for Signal Recovery

The signal output of DPN is given by $\hat{\mathbf{z}} = \hat{\mathbf{z}}_2$. This signal is already frequency compensated, noise reduced, and equalized by the network. The remaining processing that needs to be applied to this signal is the symbol recovery. This is done using the estimated timing offset \hat{t}_0 and symbol duration $\hat{\tau}$. To apply the timing recovery, the signal is interpolated by a factor of P , larger than any value of τ of interest, to get the signal $\hat{\mathbf{z}}_1$. The vector $\hat{\mathbf{z}}_1$ is padded at the start with $\hat{t}_0 P$ zeros to correct for the time offset and then sampled every $P\hat{\tau}$.

C. Symbol Decoding

The symbol decoding procedure is applied to the recovered symbols to evaluate the symbol error rate (SER) for the linear modulations. This same procedure is applied to the symbols calculated from all of the previous approaches (DPN, blind DSP, and genie). The symbols are decoded symbol per symbol, using a minimum distance euclidean receiver. A decision aided phase recovery loop uses the predicted symbol to correct the phase of the next symbol. This loop helps reduce the impact of any minor residual frequency errors. For evaluation purposes, the first symbol is assumed to be known and is used to estimate the phase to address phase ambiguity. The step-by-step procedure is described in Appendix G.

Although this approach is simple, its main disadvantage is that it propagates errors. A decision error in one symbol propagates to the remaining symbols. Since only the first symbol is used to estimate the phase in the evaluation, the initialization of the loop is subject to errors, which can propagate. More sophisticated receivers can be developed, however, we chose a simple receiver that would work for all linear modulation types. Since this receiver is common to all approaches, it should not create a bias in the evaluation.

VI. DATA GENERATION AND USRP CAPTURE

To train and test DPN, we generated a dataset consisting of signals with different data, modulation types, symbol rates, timing and frequency offsets, phase, channel impulses, and SNRs. While public datasets exist for modulation classification, they do not contain all the required signal labels, and hence are not suitable for blind decoding. In the dataset,

each signal is generated according to the flow graph shown in Fig. 4. Random data \mathbf{d} is generated and modulated using modulation type M selected from the set of single carrier modulations \mathcal{M} . If M is a linear modulation, the output is upsampled by an integer factor N_{up} and pulse shaped with a root-raised-cosine filter with a roll-off factor β . To simulate timing offsets, the first $t_0 N_{up}$ (rounded to the nearest integer) samples are removed and the signal is downsampled by a factor of $\lfloor N_{up}/\tau \rfloor$. While removing $t_0 N_{up}$ might make the first symbol unrecoverable, it is more realistic for a blind system as it emulates capturing an ongoing transmission. Since the number of removed samples and the downsampling are integers, the number of possible values of t_0 and τ is discrete and depends on N_{up} and the range of values of τ . Multipath fading is simulated using convolution with random complex fading taps having a delay spread σ . Then frequency and phase offsets, f_0 and ϕ_0 , are applied, and Gaussian noise is added to model different SNRs.

The dataset consists of signals generated with parameters uniformly sampled from the ranges shown in Table II. The upsampling factor was chosen to be equal to $N_{up} = 64$, making the number of possible values of t_0 and τ equal to 64 and 14, respectively. The channel \mathbf{h} has 3 non random zero complex taps having a Rayleigh magnitude and uniform phase. The 3 taps are spaced uniformly within the fading spread. Since single carrier modulations are more commonly used in narrowband systems with limited fading, the fading spread is assumed to be limited within one symbol duration. Unless otherwise stated, the signal length is given by $N_r = 1024$. Note that in Table II, the assumption of a sampling duration of 1 second is only made to normalize parameters and simplify the notations as stated in the system model. For a 20MHz sampling rate (50ns duration), for instance, all durations in the table should be multiplied by 50ns and the frequency offset by 20MHz.

Typically, a fixed dataset is used in training, and data augmentation is performed to avoid overfitting. Since our dataset is generated using simulations, instead of fixing the size of the training data and using augmentations, we generated the signals in real-time during training. Real-time signal generation, while eliminating overfitting, requires optimizing the generator execution time to avoid slowing down the training significantly. For training DPN, in each epoch 800K new signals are generated, the total training data for 100 epochs is 80M signals. However, note that DPN can work with a smaller fixed dataset with appropriate regularization and data augmentation similar to any other network. Also, all the networks used for comparison in this work used real-time sample generation. The validation and test sets contain a fixed 100K samples. Both sets use the same parameters given in Table II, except that the test set SNR was discretized from 0 to 20dB at 5dB steps for a more convenient result visualization.

To validate DPN's performance beyond simulations, we collected an over-the-air capture using software-defined-radios (SDRs). The capture was performed indoor using two USRP B205 mini SDRs [50] in a line-of-sight channel as shown in Fig. 5 using a center frequency of 915MHz a sampling rate of 1M samples per second ($\tau_0 = 1\mu s$). The receiver center fre-



Fig. 5: Over-the-air capture setup using USRPs B205 mini.

TABLE II: Dataset Description

Desc.	Par.	Range
Modulation Types	M	{OOK, ASK4, ASK8, OOK, ASK4, ASK8, BPSK, QPSK, PSK8, PSK16, PSK32, APSK16, APSK32, APSK64, QAM16, QAM32, QAM64, GMSK, CPFSK}
Sampling Period	τ_0	1
Frequency Offset	f_0	$[-0.01, 0.01]$
SNR (dB)	SNR	$[0, 20]$
Timing Offset	t_0	$[0, 1]$
Symbol Duration	τ	$[4, 16]$
Pulse shape rolloff	β	{0.15, 0.25, 0.35}
Phase Offset	ϕ_0	$[0, 2\pi]$
Delay Spread	σ	$[0, \tau]$

quency was intentionally offset by 5KHz (0.005Hz at $\tau_0 = 1$) to emulate the lack of prior agreement, in addition to the offsets due to the USRP oscillator accuracy having a range of $\pm 2\text{ppm}$ [50] ($\pm 1.83\text{KHz}$ at 915MHz). The Tx USRP sent 100K signals following the same modulation types and normalized symbol durations (samples per symbol) in Table II over a period of 3 minutes. The Rx USRP captured the signals, which were isolated and matched to the corresponding transmitted signals in post processing. This process was repeated three times with different signal amplitudes to obtain 3 captures with estimated SNRs equal to 8, 14, and 20dB. The SNR was estimated by measuring the received signal power and dividing it with measured power with no active transmissions. Hence, the SNR does not account for quantization noise, which is more significant for smaller signal amplitudes. The received signals, transmitted symbols, and the modulation types form the over-the-air test dataset at a given SNR.

VII. RESULTS

A. Signal Recovery

We start by evaluating the performance of DPN, SepDPN, and DSP Ref in recovering the transmitted signal. While signal recovery is not our main objective in this paper, it helps verify the merits of DPN and explain the blind decoding and modulation classification results. We start by evaluating the mean absolute error for the frequency offset \hat{f}_0 , timing offset \hat{t}_0 , and the symbol duration $\hat{\tau}$ as a function of the SNR. The mean absolute error for \hat{f}_0 is calculated using $\mathbb{E}|f_0 - \hat{f}_0|$ on the test dataset where \mathbb{E} denotes the expectation.

The results are shown in Fig. 6. In Fig. 6a, we show the original frequency offset (Orig.), which is the mean absolute value of a uniform variable from $[-0.01, 0.01]$ as stated in Table II.

We can see that for all methods the estimation error decreases as the SNR gets larger and that the residual frequency offset is lower than the original offset. Comparing the two variations of DPN, both give almost identical frequency estimation errors. This is expected since both approaches for the first frequency offset stage use only the features from the input signal. The curve for unsupDPN was omitted as it provided values above 55, which are obviously erroneous. Since unsupDPN is trained to reduce the modulation classification loss, the predicted frequency is an arbitrary value that reduces this loss with no signal processing meaning.

The DSP Ref algorithm using the parameters in the Appendices gives a higher estimation error than DPN. It is important, however, to note that DPN has the advantage of having prior information about the signals from the training data, unlike DSP Ref. The purpose of comparing to the blind DSP algorithm is just to provide a baseline reference for comparison. Each approach is considered in the way it is typically implemented and we do not claim to provide an absolute comparison between DSP algorithms in general and deep learning. This trend of results between DSP Ref and the DPN variations continues for the symbol duration and timing offset estimation. It is noteworthy that DSP Ref uses the symbol duration in the calculation of the timing offset. A mistake in the former will lead to a mistake in the latter, which would lead to a high symbol error rate in the same signal.

Then, we consider the results for the later stages of DPN; symbol duration in Fig. 6b and timing offset in Fig. 6c. We see that the proposed DPN with feature sharing performs better than the separately trained DPN, in contrast to the first stage's where the results were close. This is attributed to the fact the symbol duration and timing estimation networks of the proposed DPN, due to being at the end of the network, benefit from all the extracted features. SepDPN, on the other hand, only uses the features from the last stage. This shows that feature sharing can lead to an improvement in estimation.

The fact that the predicted estimations are close to the true values makes them reusable by signal processing algorithms. For instance, the frequency offset obtained can be used as an initial value for any carrier frequency offset tracking algorithm [43]. The symbol duration and offset can be used to initialize a symbol timing recovery algorithm [43]. This can be useful in scenarios where a long signal is received at a high sampling rate and processing the entire signal with neural networks is not computationally feasible.

Lastly, we show the recovery results on the example signal visualized in Fig. 1. For the BPSK signal having $\tau = 8$ and an SNR = 5dB and fading spread $\sigma = 0.3$, in Fig. 7, we show the power spectral density (PSD) of the input \mathbf{y} , the recovered signal $\hat{\mathbf{z}}$ from DPN, unsupDPN, and the true clean signal \mathbf{z} . These signals in time domain are visually hard to compare because of phase offsets, that is why we used the PSD. From that Figure, we can see the filter taps predicted by DPN attenuated the noise by over 25dB and made the output more similar to the truth. This shows that using only training data, DPN can predict filters that partially recover the transmitted signals. In contrast, the recovered signal from unsupDPN is arbitrary and hence has no value in blind decoding. This shows

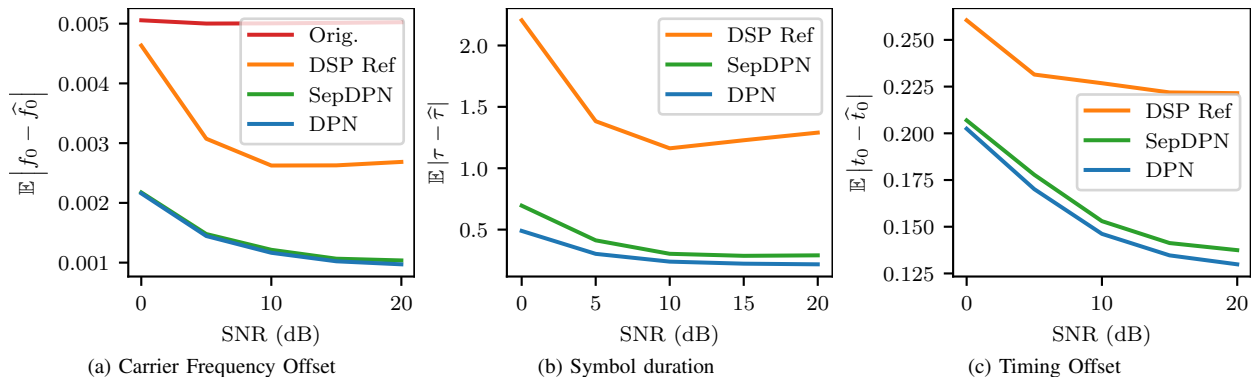


Fig. 6: The mean absolute error of DPN in parameter estimation.

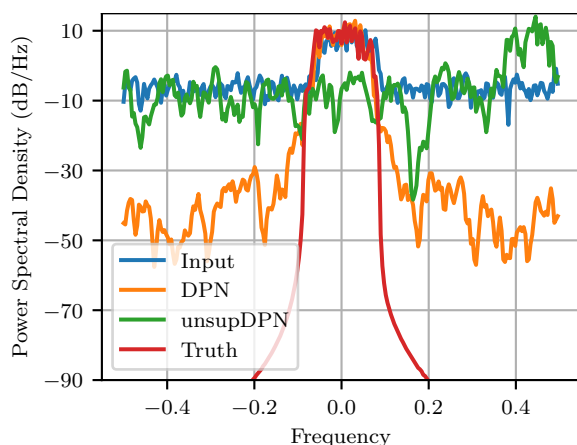


Fig. 7: The frequency representation of an example input signal, the signal recovered by DPN, and the ground truth.

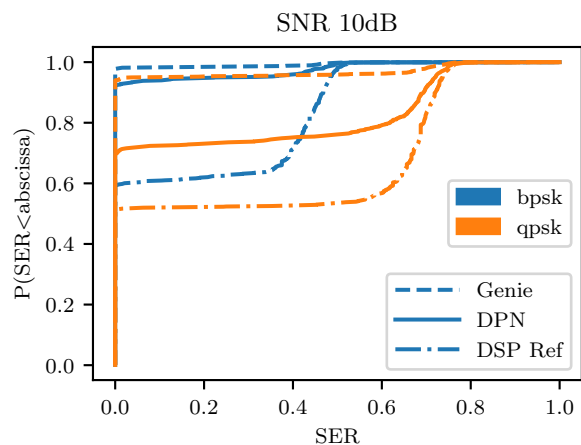


Fig. 8: The CDF of the symbol error rate (SER) calculated for each signal at SNR=10dB of different approaches.

the necessity of including the ground truth for blind decoding. Instead of evaluating the signals $\hat{\mathbf{z}}_1$ and $\hat{\mathbf{z}}_2$ over the entire dataset, which is not straight forward due to residual frequency errors, we move on to the symbol decoding evaluation. Symbol decoding implicitly evaluates the recovery stages and is our objective in this paper.

B. Blind Symbol Decoding

Then, we evaluate DPN performance in blind symbol decoding. Blindly decoding symbols is challenging since the signal parameters are not known by the blind receiver and no known preambles are assumed. Even at a high SNR, synchronization errors can lead to a high symbol error rate. Additionally, the symbol decoding procedure used in this work is relatively simple and not optimized for any specific modulation type. All these factors make obtaining a low symbol error rate (SER) as expected in a typical communication system impractical. A completely blind receiver also would not expect to obtain the same performance as a receiver with protocol knowledge.

For these reasons, we limit our results in this section to BPSK and QPSK modulations. We calculate the symbol error rate (SER) for each signal and plot the CDF of SER over all the test signals when using DPN, Genie, and DSP Ref

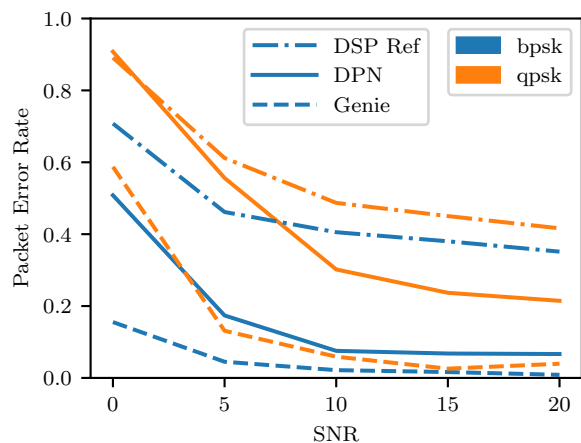


Fig. 9: The packet error rate of different approaches plotted against SNR.

for signal recovery in Fig. 8 at SNR = 10dB. DPN obtains lower SER for a larger fraction of the signals compared to Ref DSP. This follows from the fact that DPN had better results in signal recovery. As expected Genie performs better than DPN since it has access all the signal and channel parameters. Since BPSK is a lower order modulation, it can tolerate a larger

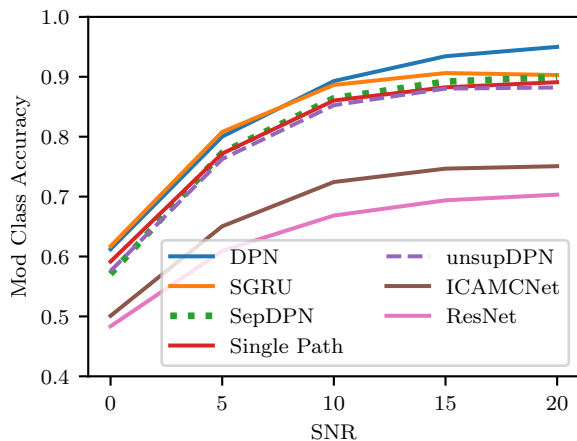


Fig. 10: The modulation classification of DPN, its alternatives SepDPN, and Single Path, and networks from the literature.

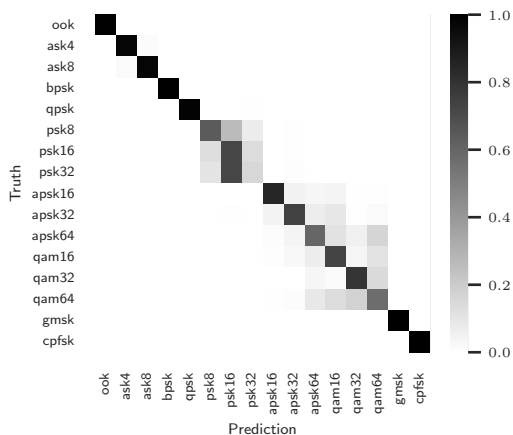


Fig. 11: The confusion matrix of DPN at SNR of 5dB.

synchronization errors and the gap between Genie and DPN is smaller for BPSK than QPSK. Notice that the CDF has a jump near SER 0.5 for BPSK and SER 0.75 for QPSK. These values are equivalent to a random guess (0.75 and not 0.5 for QPSK since we are using SER and not bit error rate). This jump is due to either a significant mistake in parameter estimation or an error in one symbol propagating to the remaining symbols in a given signal. From these results, we see that each signal is either decoded almost entirely correctly or not.

Based on this observation, we consider each signal to be a packet and consider the packet error rate (PER), equivalent to $P(\text{SER}=0)$, as a function of SNR for the same modulation types in Fig. 9. The results follow the same trend with Genie having the lowest SER followed by DPN and then DSP Ref. Since this curve is for packet error and there are between 64 and 256 symbols per packet, a random guess would yield a PER close to one. Despite that the problem of blind symbol decoding is challenging, DPN performance, while not great in absolute terms, is better than the blind DSP Ref and the PER gap between it and Genie gets as low as 5% for BPSK.

C. Modulation Classification

In this section, we consider the modulation classification performance of DPN and its variations (SepDPN, Un-supDPN,

TABLE III: Impact of each stage on Mod. Class. Accuracy

Zeroed Loss	None	L_1	L_2	L_3	L_4	L_5
Mod. Class.	83.7%	80.5%	81.6%	83.4%	83.11%	82.8%

and Single Path). We also consider networks from the literature, namely the Stacked GRU (SGRU) [12] and the ResNet [5], and ICAMCNet [24]. SGRU consists of recurrent networks and ResNet and ICAMCNet are fully convolutional networks. All networks considered are trained with real-time sample generation using the same procedures as DPN. Note that SGRU, ResNet, Single Path and un-supDPN use only the modulation type as a label in contrast to DPN and SepDPN that additionally use the frequency offset, noise reduced signal, equalized signals, and timing information. For fairness, the modulation-only networks were allowed up to 4 times the training epochs and up to 4 times the training data as DPN (up to 400 epochs and 320M training signals with early stopping).

The results are shown in Fig 10. The two networks giving the highest accuracy are DPN and SGRU. At SNR less than 10dB, both approaches yield almost the same accuracy. For SNRs larger than 10 dB, SGRU performance starts to saturate and DPN performance improves surpassing SGRU by up to 5%. This is explained by considering the signal recovery performance. At higher SNR, the signal recovery stages perform better, providing signals with less distortions for the modulation classification. Signals with less distortions result in better predictions. At lower SNR, the improvements to the signal along the signal path are more limited and do not lead to significant gains compared to SGRU. Even though DPN and SGRU attain the same accuracy below 10dB, DPN can be used for blind decoding, and is about twice faster in inference compared to SGRU as discussed later. The fully convolutional networks ICAMCNet and ResNet gave a lower accuracy than SGRU and DPN that use recurrent networks for modulation classification for this dataset having variable samples per symbol. In Fig. 11, we show the confusion matrix of DPN at 5dB SNR, from which we see that the confusion occurs mostly in high order modulations of the same type. Note that many improved deep learning layers and architectures were proposed for modulation classification in the literature. Our focus in this work is on combining DSP with deep learning and not just using improved deep learning modules for higher classification accuracy. Improved deep learning modules can easily be integrated within the dual path architecture. Hence, we focus more on interpreting DPN's design performance by comparing it with its alternative architectures.

To better understand the factors leading to DPN's results, we consider its variations. First, we see that DPN outperforms Single Path. Since Single Path consists of the exact deep-learning-based feature path of DPN, the improved results of DPN are not solely attributed to the design of the feature path. The DSP signal recovery leads to a significant accuracy improvement. To further understand the impact of each recovery stage individually on the classification, several instances of DPN were trained while setting the weight of one of the

TABLE IV: Training and Inference Times

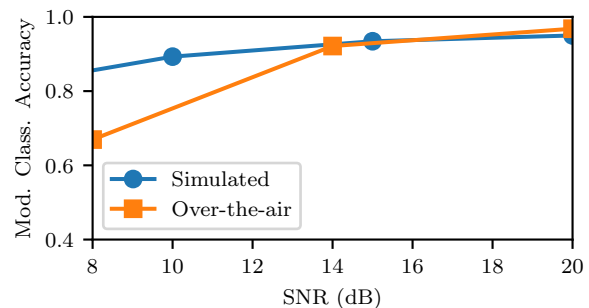
Net.	Training (s/epoch)	Inference (μ s/signal)
DPN	578.82	736
SGRU	339.22	1530
ResNet	214.52	168
ICAMCNet	227.60	135

losses L_1 to L_5 to zero. The obtained accuracies are shown in Table III. From this table, we see that eliminating the frequency correction by zeroing L_1 has the largest impact on classification, since the dataset uses high order PSK signal which are sensitive to phase shifts due to frequency errors. On the other hand, the timing offset loss L_4 has the smallest impact because of its limited impact on the signal when using more than 4 samples per symbol. Comparing DPN to SepDPN, which lacks features sharing, DPN is better at identifying the signal modulation type. Since the only advantage DPN has over SepDPN is the connection of the feature path, feature sharing that occurs along this path also contributes to the improved performance. Hence, by leveraging signal reconstruction and feature sharing, DPN design improves modulation classification by up to 5%. For unsupDPN, we see that the accuracy is also about 5% less than DPN. This result shows that including the reconstruction ground truth has the added benefit of improving the modulation classification. The similarity between the results of unsupDPN and Single Path indicates that unsupDPN was not able to leverage the reconstruction modules to improve the accuracy.

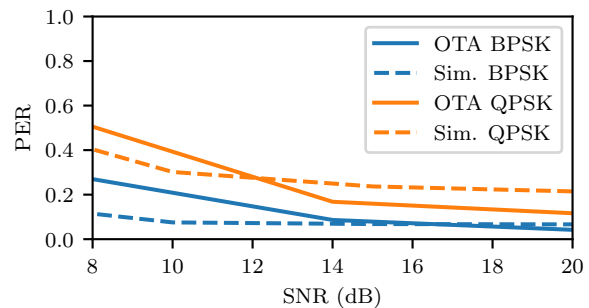
Lastly, the training and inference times of the neural networks are shown in Table IV. The training time is calculated as the average of training time per epoch. The inference time is calculated by averaging the time to make predictions per signal over the test set. The server used for calculations has an Intel Core i9-9920X (12 Cores, 3.50 GHz), an RTX 2080Ti GPU, and 128GB of RAM. From Table IV, DPN is slower to train than the other networks, since it has 6 outputs and thus requires more slow memory operations to transfer the data to the GPU for training. Note that since we are using real-time signal generation, the training time includes the overhead signal generation. In terms of inference time per signal (1024 IQ samples), DPN is slower than the fully convolutional networks (ResNet, ICAMCNet), however it is about twice faster than the SGRU. Recurrent neural networks (like SGRU and the modulation classification NN of DPN) have data dependencies among their different units, which makes them slower compared to convolutional networks. DPN consists mostly of convolutional layers except for one GRU layer much smaller than those in SGRU, and hence is faster.

D. Over-the-Air USRP Evaluation

To validate our signal model, we evaluate DPN, trained with the simulated data, using the over-the-air test dataset without any retraining. The obtained results are shown for modulation classification in Fig. 12a and packet error rate in Fig. 12b. From these Figures, we see that the OTA results



(a) Modulation Classification



(b) PER

Fig. 12: Comparison between simulation and over-the-air results

are close to the simulated datasets for the 14dB and 20dB captures². This result verifies our signal model and DPN's performance at this range of SNR. At 8dB SNR, DPN results degrade with lower modulation accuracy and higher PER. This degradation is attributed to quantization errors, which become more significant in weaker signals and has not been accounted for in the SNR estimation, along with other hardware imperfections (amplifier non-linearity, IQ imbalance, etc). These imperfections, which are typically not modeled, are known to impact RF deep learning classifiers [51]. While retraining using the OTA capture can improve performance on this specific radio capture [5], it does not guarantee that the results will generalize to different radio hardware or deployment environment and thus we do not consider it. A more in depth study of the performance trade-offs of using simulated and over-the-air data for training was performed in [51].

E. Variable Length Evaluation

As discussed earlier, DPN architecture supports using variable input lengths using the same weights. Our previous results were only for signals of length $N_r = 1024$. In this section, we evaluate the ability of DPN to generalize to lengths different than the training signals. We consider the lengths $N_r \in \{128, 256, 512, 1024, 2048\}$ for testing with 10000 signals generated at each length using a 20dB SNR. Three approaches are considered; in the first approach, we reuse the same weights θ_1 trained on signals having $N_r = 1024$

²The PER of the simulated QPSK signal is higher above 14dB because the simulated signals can have larger frequency offsets (up to 0.01Hz) compared to 0.005Hz for the OTA capture.

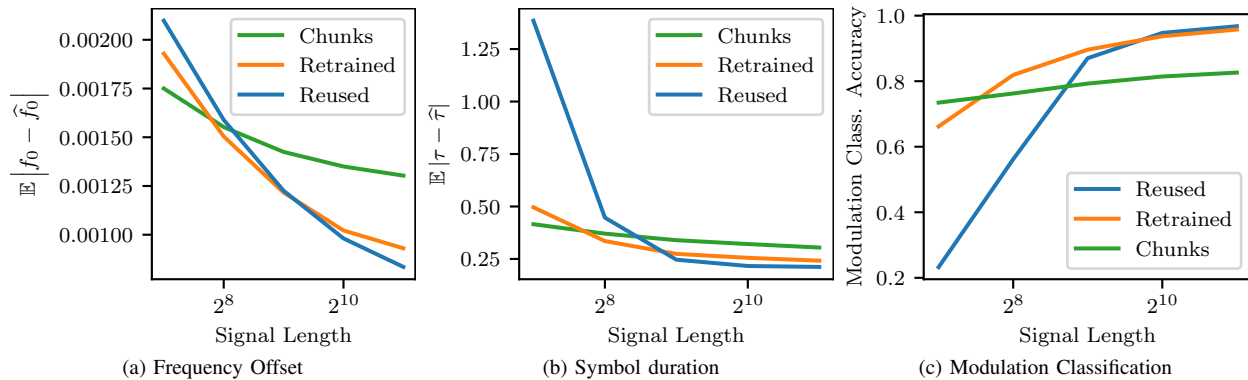


Fig. 13: Comparison of different approaches to scale DPN; dividing the signal into chunks, reusing the weights trained for $N_r = 1024$, retraining using different input lengths.

without any modifications. In the second approach, we retrain the network starting from θ_1 on signals of different lengths to obtain the weights θ_2 . The retraining was done for 20 epochs such that the signals in each training batch had a length chosen randomly within the set $\{192, 384, 768, 1536\}$, which does not overlap with the test lengths. The third approach, which works for fixed input networks, consists of training a network on the smallest input length, dividing longer signals into chunks, and averaging the predictions of each chunk as proposed in [8]. For that approach, we train DPN from scratch using signals of length 128 and predict exclusively using that length. For signals longer than 128, predictions are applied on chunks of 128 and the results are averaged.

The results for prediction errors and modulation classification are shown in Fig. 13. For all approaches, as expected the larger the signal length, the lower the estimation error and the higher the classification accuracy. Looking at the modulation classification results in Fig. 13c, reusing the weights seems to generalize well on lengths larger than 512 without any modification. For shorter lengths, however, the performance drops significantly below 60%. Retraining the weights on shorter and longer signal lengths, although different from the testing ones, does improve the performance on shorter signals as seen by looking at the retrained curve in the same Figure. This retraining, however, comes at the cost of slightly degraded performance on longer signals. The relative trend of results between retrained and reused is the same for frequency offset and symbol duration estimation. This indicates that DPN learns signal features that generalize to unseen lengths. By retraining, the weights are adjusted to improve performance on shorter signals at the expense of longer signals.

Now, looking at the curve for dividing the signal into chunks, we see that it only outperforms both the other approaches when $N_r = 128$, which is the length it was trained on. Other than that length, it provides higher estimation errors and a lower modulation classification accuracy by up to 15%. This shows that this approach is not the best way to use DPN predictions on long signals. Since the outputs \hat{f}_0 and $\hat{\tau}$ are calculated using average pooling, the degradation is not due to the averaging operation itself but to the weights learned

in training. When using only short signals in training, the learned weights extract features leveraging only short signal durations neglecting features spanning longer periods. These results highlight the benefit of DPN's design that can work using different input lengths.

VIII. CONCLUSION

In this paper, we proposed the dual path network (DPN) for blind decoding and modulation classification. DPN's design consists of three stages of signal recovery connected to form a signal path made of DSP operations and a feature path consisting of neural networks. This design enables features to be shared, enabling improved estimates in the later stages and a 5% improvement in modulation classification compared to a network separately trained. Extracting features from the recovered signals provides a 5% improvement in modulation classification compared to a similar network not recovering the signal. The estimation results of DPN are shown to outperform a reference blind DSP algorithm based on cyclostationary features. These improved estimates make it yield lower packet error rates compared to the reference algorithm. Due to the signal processing inspired design, the output filter taps and estimates are compatible with existing signal processing approaches. Using an over-the-air capture, we validated DPN results at SNRs above 14dB. By relying on average pooling and recurrent neural networks, DPN can process variable length inputs, which are shown to provide better estimates than dividing the input into short chunks and averaging.

While this work has considered blind symbol decoding, the dual path concept can be extended to other problems in wireless communications leveraging deep learning. By using a feature path consisting of neural networks and a signal path consisting of DSP operations, the outputs can be made compatible with existing signal processing approaches. Also, this design inherently enables the reuse of intermediate outputs and feature sharing, which were both shown to create a significant accuracy improvement.

APPENDIX

A. Band Segmentation

It is applied in two stages using Welch power spectral density (PSD), which consists of dividing the signal into overlapping segments, calculating the squared magnitude FFT of each segment, and averaging them. In the first stage, PSD uses an FFT of size N_1 . The occupied frequency bins are detected using a threshold T , with the edges of the occupied frequency bins given by b_1 and b_2 . The center frequency and bandwidth are calculated using $\frac{b_1+b_2}{2}$ and $\frac{b_2-b_1}{2}$, respectively. The center frequency offset is corrected and a low pass filter is applied to the signal to attenuate the noise. In the second stage, PSD is applied again with a larger FFT of size $N_2 > N_1$ to yield a higher resolution frequency and bandwidth estimate using the same procedure. Other than the FFT size, the Welch power spectral used the default parameters in the python SciPy library [52]. We used $N_1 = 64$ and $N_2 = 256$ and $T = 2N_0$.

B. Fine Carrier Frequency Estimation

The estimation of the carrier frequency is performed by detecting cyclostationary features at $\alpha = 4f_0$ [1]. Using the initial frequency estimate, a search window \mathcal{W}_{f_0} is calculated and the estimated $4f_0$ is calculated on the input signal $z[k]$ using

$$\max_{\alpha_i \in \mathcal{W}_{f_0}} \left| \sum_{k=0}^{N_f-1} z[k]^4 e^{-j2\pi \alpha_i k \tau_0} \right| \quad (7)$$

Given that the coarse frequency estimate from the prior stage was given by f_{0c} , the window \mathcal{W}_{f_0} consisted of 100 samples within $4f_0 \pm 0.001$.

C. Fine Symbol Rate Estimation

The single carrier modulations used in the evaluation have a cyclostationary feature at $\alpha = 1/\tau$, from which τ can be detected [1]. Using the coarse bandwidth estimate, a search window \mathcal{W}_τ is calculated and the estimated $1/\tau$ is calculated on the input signal $z[k]$ using

$$\max_{\alpha_i \in \mathcal{W}_\tau} \left| \sum_{k=0}^{N_s-1} |z[k]|^2 e^{-j2\pi \alpha_i k \tau_0} \right| \quad (8)$$

Given that the coarse bandwidth estimate from the prior stage was given by $1/\tau_c$, the window \mathcal{W}_τ consisted of 100 samples between $\frac{0.85}{\tau_c}$ and $\frac{1.15}{\tau_c}$.

D. Symbol Timing Offset Estimation

The input signal $z[k]$ is first interpolated by a factor of P to obtain $z_I[k]$. An error is calculated using [48]

$$e[k] = (z_I[k - P/2] - z_I[k + P/2])z_I[k]^* \quad (9)$$

where $(\cdot)^*$ denotes the conjugate. The error vector is divided into windows of size P , which are averaged across time. The timing offset index is given by the index of the zero down crossing. We used $P = 64$.

E. Blind Equalization

The CMA is an iterative blind equalization algorithm. At step m , it generates $\mathbf{w}(m)$ using stochastic gradient descent as follows [49]

$$\mathbf{w}(m) = \mathbf{w}(m-1) - \mu g(|g|^2 - 1)\mathbf{r}(m)^* \quad (10)$$

where μ is the learning rate, $g(m) = \mathbf{w}(m-1)^T \mathbf{r}(m)$, and $\mathbf{r}(m)$ is a slice of the input signal $z[k]$ starting with index m and of the same length as the filter \mathbf{w} . We used $\mu = 10^{-4}$ and an equalization filter of length 20.

F. Genie Equalization

Let $h[n]$ be the channel taps having Fourier transform $H[k]$. The frequency domain representation of the equalized signal $\hat{\mathbf{Z}}$ is given by $\hat{Z}[k] = \frac{Z[k]H^*[k]}{H^*[k]H[k]+N_0}$ where \mathbf{Z} is the FFT of the input signal. The equalized signal is obtain using the inverse FFT of $\hat{\mathbf{Z}}$.

G. Symbol Decoding

Let $\hat{\mathbf{s}}$ denote the recovered symbols before the hard decision, \mathbf{s} the true symbols, \mathbf{c}_M be the constellation of linear modulation M . The filtered phase error at the k -th symbol is denoted by $e_f[k]$. Using the assumed knowledge of the first symbol, we set $e_f[0] = \hat{s}[0]s[0]^*$. We start by calculating the constellation index of the predicted symbol $s_b[k]$ by finding the minimizer of the Euclidean distance using $s_b[k] = \text{argmin} |\hat{s}[k]e^{j e_f[k]} - \mathbf{c}_M|$, thus making the decoded symbol $s_d[k] = c_m[s_b[k]]$. The phase error $e[k]$ is calculated using the received and the decoded symbol using $e[k] = \text{arctan}(\hat{s}[k]d[k]^*)$, which is then filtered according to $e_f[k] = e_f[k] + \alpha e[k]$ for some constant α . The symbol error rate is calculated by comparing the decoded symbols \mathbf{s}_d with the true symbols \mathbf{s} . The symbol by symbol comparison is limited to the shortest of both if their lengths are different due to timing errors. We used $\alpha = 0.5$.

REFERENCES

- [1] E. Rebeiz, F.-L. Yuan, P. Urriza, D. Marković, and D. Cabric, "Energy-efficient processor for blind signal classification in cognitive radio networks," *IEEE Transactions on Circuits and Systems I: Regular Papers*, vol. 61, no. 2, pp. 587–599, 2014.
- [2] E. Kazikli, B. Dulek, and S. Gezici, "Optimal Joint Modulation Classification and Symbol Decoding," *IEEE Transactions on Wireless Communications*, vol. 18, no. 5, pp. 2623–2638, May 2019, conference Name: IEEE Transactions on Wireless Communications.
- [3] Y. Liu and F. Wang, "Blind Channel Estimation and Data Detection with Unknown Modulation and Coding Scheme," *arXiv:1909.11306 [cs, eess, math]*, Sep. 2019.
- [4] T. J. O'Shea, K. Karra, and T. C. Clancy, "Learning Approximate Neural Estimators for Wireless Channel State Information," *arXiv:1707.06260 [cs]*, Jul. 2017.
- [5] T. J. O'Shea, T. Roy, and T. C. Clancy, "Over-the-Air Deep Learning Based Radio Signal Classification," *IEEE Journal of Selected Topics in Signal Processing*, vol. 12, no. 1, pp. 168–179, Feb. 2018.
- [6] A. Balatsoukas-Stimming and C. Studer, "Deep Unfolding for Communications Systems: A Survey and Some New Directions," *arXiv:1906.05774 [cs, eess, math]*, Jun. 2019.
- [7] H. He, S. Jin, C.-K. Wen, F. Gao, G. Y. Li, and Z. Xu, "Model-Driven Deep Learning for Physical Layer Communications," *IEEE Wireless Communications*, vol. 26, no. 5, pp. 77–83, Oct. 2019.
- [8] S. Zheng, P. Qi, S. Chen, and X. Yang, "Fusion Methods for CNN-Based Automatic Modulation Classification," *IEEE Access*, vol. 7, pp. 66 496–66 504, 2019.

- [9] S. Rajendran, W. Meert, D. Giustiniano, V. Lenders, and S. Pollin, "Deep Learning Models for Wireless Signal Classification With Distributed Low-Cost Spectrum Sensors," *IEEE Transactions on Cognitive Communications and Networking*, vol. 4, no. 3, pp. 433–445, Sep. 2018.
- [10] T. Courtat and H. d. M. des Bourboux, "A light neural network for modulation detection under impairments," *arXiv:2003.12260 [cs, eess, stat]*, Mar. 2020.
- [11] T. J. O'Shea, J. Corgan, and T. C. Clancy, "Convolutional Radio Modulation Recognition Networks," *arXiv:1602.04105 [cs]*, Feb. 2016.
- [12] D. Hong, Z. Zhang, and X. Xu, "Automatic modulation classification using recurrent neural networks," in *2017 3rd IEEE International Conference on Computer and Communications (ICCC)*, Dec. 2017, pp. 695–700.
- [13] Z. Zhang, H. Luo, C. Wang, C. Gan, and Y. Xiang, "Automatic Modulation Classification Using CNN-LSTM Based Dual-Stream Structure," *IEEE Transactions on Vehicular Technology*, vol. 69, no. 11, pp. 13 521–13 531, Nov. 2020.
- [14] G. Vanhoy, N. Thurston, A. Burger, J. Breckenridge, and T. Bose, "Hierarchical Modulation Classification Using Deep Learning," in *MILCOM 2018 - 2018 IEEE Military Communications Conference (MILCOM)*, Oct. 2018, pp. 20–25.
- [15] J. Nie, Y. Zhang, Z. He, S. Chen, S. Gong, and W. Zhang, "Deep Hierarchical Network for Automatic Modulation Classification," *IEEE Access*, vol. 7, pp. 94 604–94 613, 2019.
- [16] S. Chen, Y. Zhang, Z. He, J. Nie, and W. Zhang, "A Novel Attention Cooperative Framework for Automatic Modulation Recognition," *IEEE Access*, vol. 8, pp. 15 673–15 686, 2020.
- [17] S. Peng, H. Jiang, H. Wang, H. Alwageed, Y. Zhou, M. M. Sebdani, and Y.-D. Yao, "Modulation Classification Based on Signal Constellation Diagrams and Deep Learning," *IEEE Transactions on Neural Networks and Learning Systems*, vol. 30, no. 3, pp. 718–727, Mar. 2019.
- [18] S. Huang, Y. Jiang, Y. Gao, Z. Feng, and P. Zhang, "Automatic Modulation Classification Using Contrastive Fully Convolutional Network," *IEEE Wireless Communications Letters*, pp. 1–1, 2019.
- [19] S. Huang, L. Chai, Z. Li, D. Zhang, Y. Yao, Y. Zhang, and Z. Feng, "Automatic Modulation Classification Using Compressive Convolutional Neural Network," *IEEE Access*, vol. 7, pp. 79 636–79 643, 2019.
- [20] V.-S. Doan, T. Huynh-The, C.-H. Hua, Q.-V. Pham, and D.-S. Kim, "Learning Constellation Map with Deep CNN for Accurate Modulation Recognition," *arXiv:2009.02026 [cs, eess, math]*, Sep. 2020.
- [21] S. Ramjee, S. Ju, D. Yang, X. Liu, A. E. Gamal, and Y. C. Eldar, "Fast Deep Learning for Automatic Modulation Classification," *arXiv:1901.05850 [cs, eess, stat]*, Jan. 2019.
- [22] —, "Ensemble Wrapper Subsampling for Deep Modulation Classification," *arXiv:2005.04586 [cs, eess, stat]*, May 2020.
- [23] Z. Ke and H. Vikalo, "Real-Time Radio Technology and Modulation Classification via an LSTM Auto-Encoder," *arXiv:2011.08295 [cs, eess]*, Nov. 2020.
- [24] A. P. Hermawan, R. R. Ginanjar, D.-S. Kim, and J.-M. Lee, "CNN-Based Automatic Modulation Classification for Beyond 5G Communications," *IEEE Communications Letters*, pp. 1–1, 2020.
- [25] H. Zhang, Y. Wang, L. Xu, T. Aaron Gulliver, and C. Cao, "Automatic Modulation Classification Using a Deep Multi-Stream Neural Network," *IEEE Access*, vol. 8, pp. 43 888–43 897, 2020.
- [26] k. Liao, G. Tao, Y. Zhong, Y. Zhang, and Z. Zhang, "Sequential Convolutional Recurrent Neural Networks for Fast Automatic Modulation Classification," *The Astrophysical Journal*, vol. 878, no. 1, p. 6, Jun. 2019.
- [27] T. Xu and I. Darwazeh, "Deep Learning for Over-the-Air Non-Orthogonal Signal Classification," *arXiv:1911.06174 [cs, eess]*, Nov. 2019.
- [28] L. Li, Q. Peng, and J. Wang, "Deep Architectures for Modulation Recognition with Multiple Receive Antennas," *arXiv:2008.06720 [cs, eess, math]*, Aug. 2020.
- [29] W. Jiang, X. Wu, B. Chen, W. Feng, and Y. Jin, "Time-Frequency Analysis based Blind Modulation Classification for Multiple-Antenna Systems," *arXiv:2004.00378 [cs, eess, stat]*, Apr. 2020.
- [30] L. J. Wong, P. White, M. Fowler, and W. C. Headley, "Distributed Automatic Modulation Classification with Compressed Data," in *MILCOM 2019 - 2019 IEEE Military Communications Conference (MILCOM)*, Nov. 2019, pp. 299–304.
- [31] S. C. Hauser, W. C. Headley, and A. J. Michaels, "Signal detection effects on deep neural networks utilizing raw IQ for modulation classification," in *MILCOM 2017 - 2017 IEEE Military Communications Conference (MILCOM)*, Oct. 2017, pp. 121–127.
- [32] M. Mirmohammadsadeghi, S. S. Hanna, and D. Cabric, "Modulation classification using convolutional neural networks and spatial transformer networks," in *2017 51st Asilomar Conference on Signals, Systems, and Computers*, Oct. 2017, pp. 936–939.
- [33] T. J. O'Shea, L. Pemula, D. Batra, and T. C. Clancy, "Radio Transformer Networks: Attention Models for Learning to Synchronize in Wireless Systems," *arXiv:1605.00716 [cs]*, May 2016.
- [34] K. Yashashwi, A. Sethi, and P. Chaporkar, "A Learnable Distortion Correction Module for Modulation Recognition," *arXiv:1803.01319 [eess]*, Mar. 2018.
- [35] X. Shang, H. Hu, X. Li, T. Xu, and T. Zhou, "Dive into Deep Learning Based Automatic Modulation Classification: A Disentangled Approach," *IEEE Access*, pp. 1–1, 2020.
- [36] S. Zheng, X. Zhou, S. Chen, P. Qi, and X. Yang, "DemodNet: Learning Soft Demodulation from Hard Information Using Convolutional Neural Network," *arXiv:2011.11337 [eess]*, Nov. 2020.
- [37] Y. Zhang, A. Doshi, R. Liston, W.-t. Tan, X. Zhu, J. G. Andrews, and R. W. Heath, "DeepWiPHY: Deep Learning-based Receiver Design and Dataset for IEEE 802.11ax Systems," *arXiv:2010.09268 [cs, eess]*, Oct. 2020.
- [38] M. Honkala, D. Korpi, and J. M. J. Huttunen, "DeepRx: Fully Convolutional Deep Learning Receiver," *arXiv:2005.01494 [cs]*, Jan. 2021.
- [39] S. Dörner, S. Cammerer, J. Hoydis, and S. t Brink, "Deep Learning Based Communication Over the Air," *IEEE Journal of Selected Topics in Signal Processing*, vol. 12, no. 1, pp. 132–143, Feb. 2018.
- [40] T. J. O'Shea, K. Karra, and T. C. Clancy, "Learning to communicate: Channel auto-encoders, domain specific regularizers, and attention," in *2016 IEEE International Symposium on Signal Processing and Information Technology (ISSPIT)*, Dec. 2016, pp. 223–228.
- [41] T. J. O'Shea, T. Erpek, and T. C. Clancy, "Deep Learning Based MIMO Communications," *arXiv:1707.07980 [cs, math]*, Jul. 2017.
- [42] S. Hanna, C. Dick, and D. Cabric, "Combining Deep Learning and Linear Processing for Modulation Classification and Symbol Decoding," *arXiv:2006.00729 [eess]*, Jun. 2020.
- [43] F. Harris, "Let's Assume the System Is Synchronized," in *Globalization of Mobile and Wireless Communications*. Dordrecht: Springer Netherlands, 2011, pp. 311–325.
- [44] S. S. Hanna, A. A. El-Sherif, and M. Y. ElNainay, "Maximizing USRP N210 SDR transfer rate by offloading modulation to the on-board FPGA," in *2016 International Conference on Wireless Networks and Mobile Communications (WINCOM)*, Oct. 2016, pp. 110–115.
- [45] I. Goodfellow, Y. Bengio, and A. Courville, *Deep Learning*. MIT Press, 2016.
- [46] K. He, X. Zhang, S. Ren, and J. Sun, "Deep Residual Learning for Image Recognition," *arXiv:1512.03385 [cs]*, Dec. 2015.
- [47] R. Pascanu, T. Mikolov, and Y. Bengio, "On the difficulty of training recurrent neural networks," in *Proceedings of the 30th International Conference on International Conference on Machine Learning - Volume 28*, ser. ICML'13. Atlanta, GA, USA: JMLR.org, Jun. 2013, pp. III–1310–III–1318.
- [48] F. M. Gardner, "A BPSK/QPSK timing-error detector for sampled receivers," *IEEE Transactions on Communications*, vol. 34, pp. 423–429, 1986.
- [49] Q. Shi, "Blind equalization and characteristic function based robust modulation recognition," in *2012 14th International Conference on Advanced Communication Technology*, Feb. 2012, pp. 660–664.
- [50] Ettus Research, "USRP B205mini-i," <https://www.ettus.com/all-products/usrp-b205mini-i/>.
- [51] W. H. Clark IV, S. Hauser, W. C. Headley, and A. J. Michaels, "Training Data Augmentation for Deep Learning RF Systems," *arXiv:2010.00178 [cs, eess]*, Sep. 2020.
- [52] P. Virtanen, R. Gommers, T. E. Oliphant, M. Haberland, T. Reddy, D. Cournapeau, E. Burovski, P. Peterson, W. Weckesser, J. Bright, S. J. van der Walt, M. Brett, J. Wilson, K. J. Millman, N. Mayorov, A. R. J. Nelson, E. Jones, R. Kern, E. Larson, C. J. Carey, Í. Polat, Y. Feng, E. W. Moore, J. VanderPlas, D. Laxalde, J. Perktold, R. Cimrman, I. Henriksen, E. A. Quintero, C. R. Harris, A. M. Archibald, A. H. Ribeiro, F. Pedregosa, P. van Mulbregt, and SciPy 1.0 Contributors, "SciPy 1.0: Fundamental algorithms for scientific computing in python," *Nature Methods*, vol. 17, pp. 261–272, 2020.